Friction **12**(3): 474–489 (2024)
https://doi.org/10.1007/s40544-023-0776-0
ISSN 2223-7690
CN 10-1237/TH
RESEARCH ARTICLE

Tribological properties and tribomechanism of nickel nanoparticles *in-situ* synthesized in rapeseed oil

Wenya XU[1], Guangbin YANG[1,*], Shengmao ZHANG[1], Jun XU[2], Yujuan ZHANG[1], Tianhua SUN[1], Ningning SONG[1], Laigui YU[1], Pingyu ZHANG[1,*]

[1] *Engineering Research Center for Nanomaterials, Henan University, Kaifeng 475004, China*

[2] *State Key Laboratory of Tribology in Advanced Equipment, Tsinghua University, Beijing 100084, China*

Received: 25 August 2022 / Revised: 13 October 2022 / Accepted: 03 May 2023

Abstract: Nickel (Ni) nanoparticles can be enriched on the surface of iron-based frictional pairs, which provides the possibility to get rid of the competitive adsorption between the polar species of vegetable oil and the surface-active nano-additives thereon. In this paper, nickel acetylacetonate was used as a precursor to *in-situ* synthesize nickel nanoparticles with an average diameter of about 12 nm in rapeseed oil (RO) as the reducing agent, surface modifier, and solvent as well. The tribological properties of the as-synthesized Ni nanoparticles were evaluated with a four-ball tribometer, and their tribomechanism was investigated based on the characterizations of the tribofilm on rubbed steel surfaces by the scanning electron microscopy (SEM), transmission electron microscopy (TEM), and X-ray photoelectron spectroscopy (XPS). It was found that the Ni nanoparticles *in-situ* prepared in the RO with a mass fraction of 0.3% can reduce the wear scar diameter (WSD) of the steel ball by 36%. This is because, on the one hand, the Ni nanoparticles are adsorbed on the rubbed steel surfaces to repair or fill up the micro-pits and grooves thereon. On the other hand, Ni nanoparticles participate in tribochemical reactions with atmospheric O and steel substrate to form the tribochemical reaction film on the rubbed steel surfaces with the assistance of friction-induced heat and applied normal load. In addition, an amorphous carbon film is formed on the rubbed surface via the carbonization of base oil under the catalysis of Ni nanoparticles. The adsorbed Ni layer, the tribochemical reaction film, and the carbon layer comprise a composite tribofilm composed of amorphous carbon, polar fatty acid, metallic nickel, iron oxides, and nickel oxides on the rubbed steel surfaces, which contributes to significantly improving the antiwear ability and load-carrying capacity of the RO for the steel–steel sliding pair.

Keywords: nickel (Ni) nanoparticles; rapeseed oil (RO); *in-situ* synthesis; tribological properties; tribomechanism

1 Introduction

With the increasing attention to environmental protection worldwide, the demand for environment-friendly lubricants will inevitably continue to increase [1–5]. Therefore, the exploration, development, and application of environment-friendly lubricants are required for the sustainable development of human society. However, environment-friendly lubricants are facing a variety of concerns in engineering, mainly due to their fair tribological properties and biodegradability as well as undesired toxicity.

Vegetable oils, mainly composed of saturated fatty acids with 12–18 carbons and unsaturated fatty acids with 1–3 double bonds, have excellent biodegradability and are potential base stocks of environment-friendly lubricants. The unsaturated fatty acids, unfortunately, may deteriorate the thermo-oxidative stability of vegetable oils and reduce their lubrication efficiency [6–8]. Therefore, it is urgent to seek for novel

* Corresponding authors: Guangbin YANG, E-mail: yang0378@henu.edu.cn; Pingyu ZHANG, E-mail: pingyu@henu.edu.cn

high-performance lubricant additives in order to improve the thermo-oxidative stability and lubricity of vegetable oils. In this respect, nanoparticles without phosphorus, sulfur, and other environment-unfriendly triboactive elements are of particular significance, since they could improve the tribological properties of base oil through sliding, rolling, polishing, filling, and other lubrication mechanisms or participating in tribochemical reactions [9–12]. Karthikeyan et al. [13] reported that the dispersions of MoS_2 (0.7%, mass fraction) in castor oil and olive oil can reduce the wear of pin-on-disc contact to some extent but have nearly no effect on the friction-reducing ability of the two kinds of base oil. Alves et al. [14] claimed that ZnO and CuO nanoparticles as the additives in vegetable base lubricants (such as soybean oil and sunflower oil) are not beneficial to wear reduction, possibly due to the competitive adsorption of the polar vegetable oil on the rubbed metal surface. In other words, the polar fatty acid in vegetable oil competes with nanoparticles in terms of their adsorption on the rubbed metal surface, which makes nanoparticles exert the third-body behavior and undergo antagonism with the vegetable oil, thereby damaging the tribological properties of the lubricants.

This drawback of nanoparticles, fortunately, could be eliminated by incorporating proper organic molecules onto the surface of nanoparticles to achieve surface chemical modification. Chen et al. [15] pointed out that the encapsulation of cerium borate nanoparticles with stearic acid contributes to improving the friction-reducing and antiwear properties of rapeseed oil (RO). The reason lies in that the surface-capped cerium borate nanoparticles and the polar species of RO are jointly adsorbed on the rubbed metal surface, while they also take part in tribochemical reactions to form a composite boundary lubricating film composed of CeO_2, Fe_2O_3, etc. Jiang et al. [16, 17] carried out secondary modification of oleylamine-modified WS_2 nanoparticles with maleic anhydride monododecyl ester, and they successfully improved the surface polarity of the WS_2 nanoparticles and the tribological properties of ester oils by making use of the dual surface-modification technique. However, the introduction of the polar modifier often leads to significant increases in the polarity of the nanoparticles and the acid value of the lubricating oil, which is unfavorable for reducing the corrosion and wear of the frictional pair. This reminds us that it could be essential to getting rid of the negative influences of the surface modifiers applicable to *in-situ* surface-modification of inorganic nanoparticles.

Because of the unique magnetism properties, nickel (Ni) nanoparticles as lubricant additives are easily adsorbed on the surface of frictional pair to form a protective film, thereby greatly improving the antiwear performance of the base oil. Meng et al. [18] synthesized a nickel/multi-walled carbon nanotube nanocomposite as a lubricant additive through the chemical reduction route in a supercritical carbon dioxide fluid, and they found that the as-synthesized nanocomposite dispersed in 500N mineral oil with a concentration of about 0.20% contributes to reducing the coefficient of friction (COF) and wear rate by 44.2% and 56.4%, respectively. Tu et al. [19] reported that the carbon quantum dot-doped nickel (Ni–CQD) as an additive can significantly reduce the friction and wear of polyethylene glycol, which is related to the formation of a tribofilm upon tribochemical reactions of Ni–CQD. We found in Refs. [20, 21] that ellipsoidal and cubic nickel nanoparticles modified by oleylamine as the additives for poly-alpha-olefin (PAO) and diisooctylsebacate (DIOS) base oils can significantly reduce the COFs and wear rates of steel–steel sliding pairs. More importantly, the surface-capped Ni nanoparticles as the additive of the polar DIOS base oil show an obvious negative wear phenomenon and can *in-situ* repair the worn steel surfaces under a magnetic field.

Currently available methods for preparing nickel nanoparticles mainly cover physical routes and chemical routes. Commonly used physical methods for preparing Ni nanoparticles mainly include the plasma method [22], ultrasonic-aided electrical discharge erosion method [23], and high-energy ball milling method [24], but these methods have obvious disadvantages such as high cost, large sample size, as well as easy oxidation, uneven particle size distribution, and easy agglomeration of product. The representative chemical methods are the liquid reduction method [25] and thermal decomposition method [26]. The target products prepared by the liquid reduction method

have a low yield and are easy to agglomerate, while those obtained by the thermal decomposition method require higher reaction temperatures and often accompany by environmentally unacceptable by-products. Since traditional preparation methods of nickel nanoparticles are usually complicated and less cost-effective in association with poor environmental acceptance, it is imperative to establish environment-friendly, facile, and easily-scalable route to fabricating nickel nanoparticles [27].

In this research, nickel nanoparticles were *in-situ* synthesized in RO by a simple and convenient liquid-phase method. With nickel acetylacetonate as the nickel source and RO as the reducing agent as well as the modifier and solvent, the as-synthesized product can be directly used as the RO-based lubricant additive, which is favorable for reducing the cost and for environmental protection as well. This paper deals with the preparation of the Ni nanoparticles via the *in-situ* reduction of nickel acetylacetonate in RO. Aiming at providing new opportunities for the development and application of vegetable oil-based nanolubricants, it also discusses the tribological properties and lubrication mechanism of the as-synthesized nickel nanoparticles in relation to worn surface characterizations by a variety of modern analytical facilities.

2 Experimental

2.1 Chemicals

Nickel acetylacetonate (analytical grade) was supplied by Shanghai Aladdin Biochemical Technology Co. Ltd. RO (food grade) was ordered from Shanghai Fulinmen Food Co. Ltd. Analytical grade n-hexane was provided by Tianjin Kermel Chemical Reagent Co. Ltd. All chemicals were directly used without further purification.

2.2 *In-situ* synthesis of nickel nanoparticles in RO

The schematic diagram for the *in-situ* synthesis of Ni nanoparticlesin RO is displayed in Fig. 1. In brief, 0.38 g of nickel acetylacetonate and 30 mL of RO are poured into a 50 mL three-necked flask and heated with an electric heating jacket at a heating rate of 5 °C/min. Under mechanical stirring and nitrogen protection, the color of the solution gradually changes from green to yellow in the temperature range of 120–135 °C and from yellow to black in the temperature range of 135–190 °C, and it turns into black completely after being held at 200 °C for 30 min. At the end of the reaction, the black solution is centrifuged and washed three times with n-hexane to obtain black Ni nanoparticles, the target product denoted as RO–Ni.

2.3 Characterization

The as-prepared nickel nanoparticles were characterized by the X-ray diffraction (XRD; DX-2700BH, Haoyuan Instruments, China; operating at 40 kV and 30 mA over the 2θ range of 35°–85°) with Cu-Kα radiation as the excitation source. The morphologies of nickel nanoparticles were examined by a transmission electron microscopy (TEM; JEM2100Plus, JEOL, Japan) working at 200 kV, and the statistical analysis of the particle size based on the TEM photographs was conducted with the Nano Measurer software (Version 1.2, Fudan

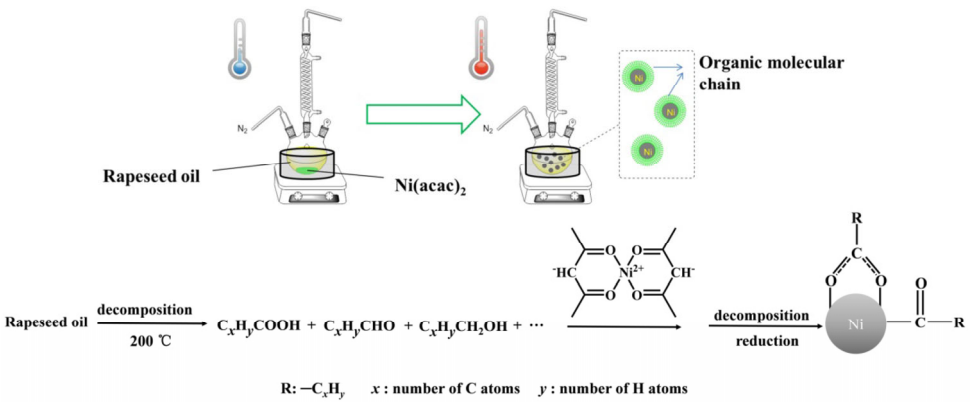

Fig. 1 Schematic diagram of nickel nanoparticles *in-situ* synthesized in rapeseed oil.

University, China). Their chemical features were analyzed by the Fourier transform infrared (FTIR) spectroscopy (VERTEX 70, Bruker, Germany), and their thermal stability was evaluated by the thermogravimetric analysis (TGA) from room temperature to 700 °C at a heating rate of 10 °C/min under a nitrogen atmosphere.

2.4 Friction and wear tests

The tribological properties of the as-prepared Ni nanoparticles in RO were determined by a four-ball tribometer (MS-10A, Tenkey China). As shown in Fig. 2, the antiwear ability of RO–Ni is evaluated by measuring the average diameter of the circular wear scar on the three bottom stationary balls with a charge-coupled device (CCD) sensor, and its lubricating performance is evaluated by monitoring the produced friction torque. The GCr15 steel balls with an elastic modulus of 207 GPa, a reduced elastic modulus (E') of 228 GPa, and a Poisson's ratio of 0.30 were used to assemble the steel–steel sliding pair. According to the Chinese Petrochemical Industry Standard NB/SH/T 0189-2017, the sliding tests were run at a rotation speed of 1,200 r/min and a normal load of 392 N (Hertzian pressure: 2.30 GPa) for 60 min. Each sliding test was repeated for at least 3 times, and the average values were calculated and reported in this article. The COF was measured and recorded automatically by the software of the test rig, and the wear scar diameters (WSDs) of the three bottom balls were measured with the CCD sensor. Moreover, the steel balls were fully cleaned with petroleum ether under an ultrasonic vibration and used for characterizations.

A white light interferometer (CounterGT-K, Bruker, Germany) was performed to analyze the three-dimensional (3D) morphologies of the wear scars. The morphologies and element compositions of the worn steel surfaces were analyzed by the scanning electron microscopy (SEM; Gemini SEM 500, Carl Zeiss, USA) equipped with an energy dispersive spectroscopy (EDS) accessory. An X-ray photoelectron spectroscopy (XPS; ESCALAB 250Xi, Thermo Scientific, USA) was used to analyze the chemical composition and chemical state of the tribofilm formed on the worn steel surface, and the binding energy of the carbon contaminant (C 1s: 284.8 eV) was used as a reference. A focused ion beam (FIB) system was employed to prepare the cross-sectional sample of the tribofilm on the wear scar, and the wear scar was ion plated with a Pt layer so as to get rid of the damage to the tribofilm upon the FIB processing. Moreover, the structure and chemical composition of the tribofilm were examined by the TEM equipped with an EDS attachment.

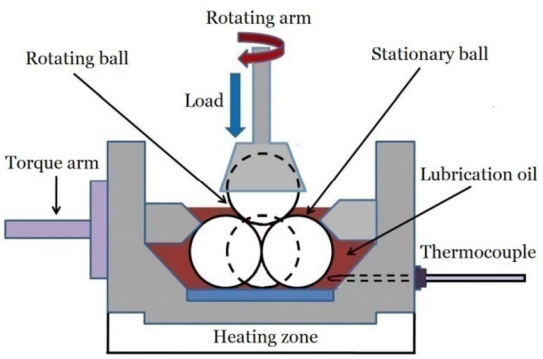

Fig. 2 Schematic of four-ball tribometer.

3 Results and discussion

3.1 Characterization of nickel nanoparticles

Figure 1 schematically presents the *in-situ* synthesis of Ni nanoparticles in RO. A major highlight of the present approach is that it adopts RO as the reducing agent, modifier, and solvent as well. With the increasing reaction temperature and time, the fatty acid chains of RO may break apart, producing a series of shorter chain aldehydes, ketones, alcohols, acids, and other decomposition products [28, 29]; some decomposition products such as aldehydes and alcohols act as the reducing agents. This makes it feasible to *in-situ* reduce nickel acetylacetonate precursor into Ni nanoparticles in a facile and green manner, which could be particularly valuable for the development of novel high-performance green lubricants, thanks to the desired biodegradability, environmentally friendliness, abundance, and good availability of RO. After the introduction of nickel acetylacetonate, the light yellow RO turns into green, and the color of the reaction solution further turns to yellow and black gradually with the increasing reaction temperature. Upon completion of reaction, the RO containing 0.3% (mass fraction) Ni nanoparticles remains uniform and black and shows no sign of precipitation after

being left undisturbed at room temperature for 20 d, and the as-synthesized Ni nanoparticles have a certain degree of response to external magnets (Fig. 3). This indicates that they exhibit good dispersion stability in the RO and some magnetism as well.

Figure 4 shows the typical XRD pattern of the *in-situ* synthesized nickel nanoparticles in RO. A comparison with the standard card (PDF#87-0712) in Raney Ni demonstrates that the *in-situ* synthesized Ni nanoparticles can be assigned to a face-centered cubic (fcc) nickel structure, and their diffraction peaks at 44.57°, 51.88°, and 76.45° are ascribed to the (111), (200), and (220) crystal planes of the fcc-Ni, respectively [30, 31]. This means that the nickel nanoparticles *in-situ* synthesized in RO consist of a highly pure fcc-Ni crystal. In addition, the XRD spectrum was fitted by Origin software (Pro 9.0, OriginLab, USA) to obtain the full width at half maximum (FWHM, β) of each peak (0.8563, 1.3517, and 1.4093 rad), and then the average crystal size (D) is calculated to be 7.9 nm according to the Scherrer equation (Eq. (1)).

$$D = \frac{K\delta}{\beta\cos\theta} \tag{1}$$

where K (taken as 0.9) is the Scherrer constant, δ (= 0.15406 nm) is the wavelength of the X-ray source, and θ is the peak position (in rad).

The as-synthesized nickel nanoparticles are of a spherical shape, and their average particle diameter increases with the increasing reaction temperature. When the reaction temperature exceeds 210 °C, the as-obtained Ni nanoparticles have a relatively broad particle size distribution and tend to agglomerate at a certain degree (Fig. S1 in the Electronic Supplementary Material (ESM)). Furthermore, with the increase of the reaction time, the particle size also increases gradually, due to the Ostwald ripening phenomenon (Fig. S2 in the ESM). Based on a series of comparative tests, the optimized reaction temperature and time for the *in-situ* synthesis of Ni nanoparticles are determined to be 200 °C and 30 min, respectively. Figure 5 presents the TEM images and particle size distribution of nickel nanoparticles prepared under the optimal reaction condition. It can be seen that they exhibit an average particle size of 12.2 nm as well as a narrow particle size distribution and good dispersibility. This could be because the high content of polar fatty acids in RO not only functions to modify the surface of nickel nanoparticles but also limits the growth and agglomeration of Ni nanocrystal during the *in-situ* reduction of nickel acetylacetonate by RO. Furthermore, the average particle size obtained by the TEM method is larger than the D determined by means of the XRD method, indicating that the as-prepared Ni nanoparticles are not single crystals, and the particles observed by the TEM are composed of multiple crystal grains.

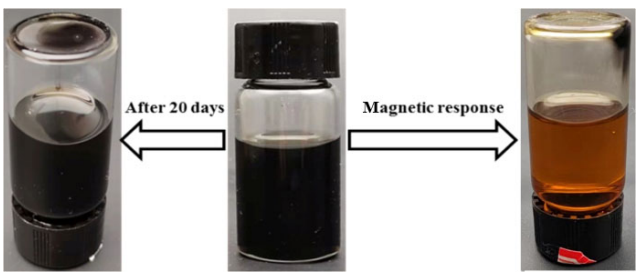

Fig. 3 Optical microscopic images of rapeseed oil containing 0.3% Ni nanoparticles.

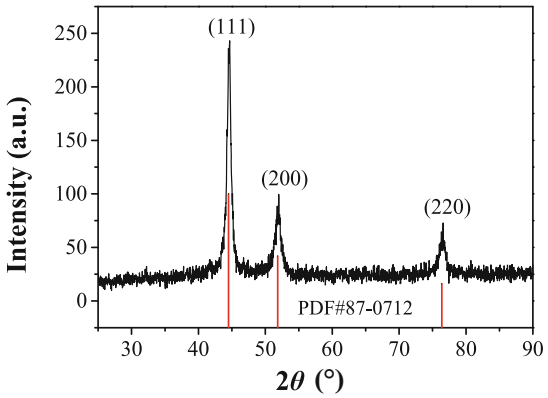

Fig. 4 XRD pattern of nickel nanoparticles *in-situ* synthesized in rapeseed oil.

The FTIR analysis of Ni nanoparticles and RO is carried out to analyze their chemical compositions. As shown in Fig. 6, the absorbance peak at 3,471.6 cm^{-1} is attributed to the stretching vibration of the dimerized hydroxyl (–OH) of RO, the absorbance peaks at 2,946.6 and 2,857.3 cm^{-1} correspond to the methyl ($–CH_3$) and methylene ($–CH_2–$) stretching vibrations of RO, respectively, and the bending vibration of C–H at 1,456.0 cm^{-1} was due to the presence of $–CH_3$. Besides, the absorbance peak at 1,745.4 cm^{-1} is assigned to C=O, and the peak at 1,161.3 cm^{-1} corresponds to the C–O stretching vibration in saturated aliphatic,

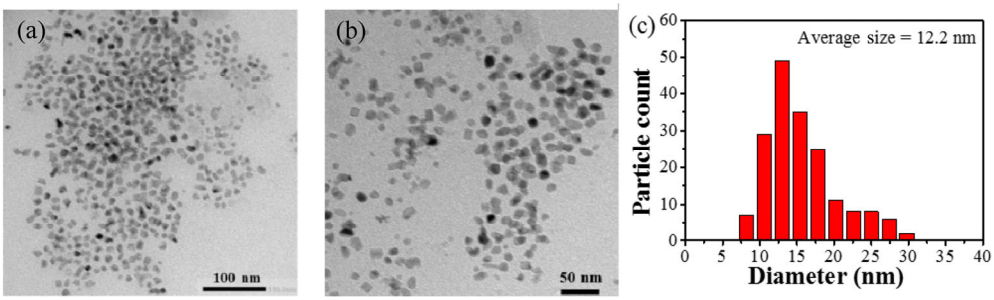

Fig. 5 TEM images and particle size distribution of Ni nanoparticles *in-situ* synthesized in rapeseed oil.

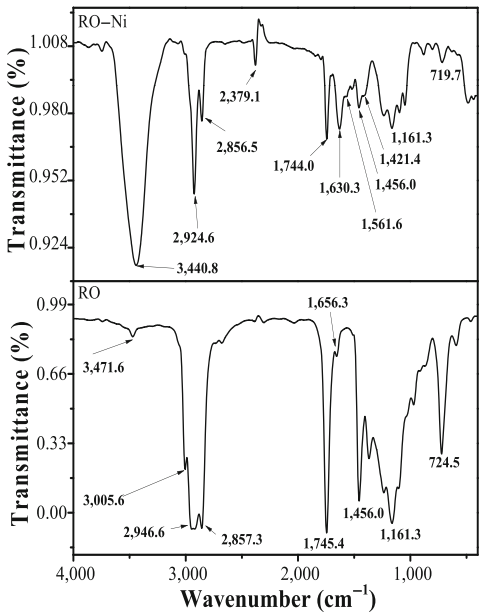

Fig. 6 FTIR spectra of nickel nanoparticles *in-situ* synthesized in rapeseed oil.

indicating the presence of ester bonds. The peak at 1,656.3 cm^{-1} is ascribed to the stretching vibration of C=C [32], and the peak at 724.5 cm^{-1} corresponds to the in-plane rocking vibrations of –$(CH_2)_n$– (n is equal to and above 4) [33, 34]. This proves that the RO is mainly composed of saturated and unsaturated fatty acids. Different from that in the FTIR spectrum of RO, the intensity of the peak at 1,744.0 cm^{-1} in the FTIR spectrum of Ni nanoparticles is significantly weaker than that of the peak at 1,745.4 cm^{-1} in RO, which indicates the cleavage of the ester bond in the triglyceride structure. Furthermore, two new bands at 1,561.6 and 1,421.4 cm^{-1} appeared, and thus they were attributed to the asymmetric –COO^- and symmetric –COO^- stretching vibration bands, respectively. These results confirm that the carboxyl groups in RO are chemically bonded to the surface of the Ni metal to form mono-dentate carboxylates or bidentate carboxylates [35, 36].

The TGA curve of the nickel nanoparticles *in-situ* synthesized in RO is presented in Fig. 7. It is also divided into three stages according to the thermal decomposition of RO (Fig. S3 in the ESM) [37]: In the first stage, the nickel nanoparticles have an obvious weight loss in the temperature range of 288–380 °C, in which the weight loss of 31% is attributed to the decomposition of the polyunsaturated fatty acid modified on the surface of nickel nanoparticles. The slow weight loss (about 7%) at the second stage in the temperature range of 380–480 °C is due to the decomposition of monounsaturated fatty acids. And the third decomposition stage in the temperature range of 480–560 °C is related to the thermal decomposition of the saturated fatty acids; when the temperature exceeds 560 °C, the TGA curve is similar to that of RO (Fig. S3 in the ESM) and remains stable, which indicates that the organic species on the surface of the Ni nanoparticles are completely decomposed thereat. From the thermal analysis results, the content of the fatty acid on the surface of the *in-situ* synthesized nickel nanoparticles in RO is estimated to be 44%.

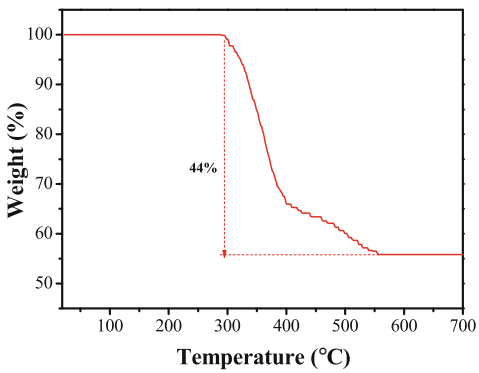

Fig. 7 TGA curve of nickel nanoparticles *in-situ* synthesized in rapeseed oil.

3.2 Tribological properties

Figure 8 presents the COFs and WSDs of the steel–steel contact under the lubrication of RO with 0.3% nickel nanoparticles prepared at different reaction temperatures (the reaction time is fixed at 30 min). Compared with neat RO, the RO containing 0.3% Ni nanoparticles prepared at different temperatures lead to a certain degree of the increase in the COF (Fig. 8(a)). Namely, the average COF under the lubrication of RO is about 0.064 (Fig. 8(b)), and that under the lubrication of RO with 0.3% nickel nanoparticles prepared at different reaction temperatures (190–220 °C, at an interval of 10 °C) is around 0.090 (increased by about 40%, as compared with the one for RO alone). This could be because the Ni nanoparticles and the RO base oil are adsorbed and deposited on the rubbed steel surface to generate a boundary lubrication film with higher shear strength and/or surface roughness than the steel substrate [38]. Besides, the as-synthesized Ni nanoparticles with a dosage of 0.3% in the RO exhibit improved antiwear performance for the steel–steel contact (Fig. 8(c)), and the Ni nanoparticles *in-situ* synthesized in the RO under reaction temperatures of 200, 210, and 220 °C have similar antiwear ability therein. This could still be due to the deposition of nickel nanoparticles on the rubbed surfaces of the steel–steel contact. Namely, the as-deposited Ni nanoparticles function to fill up the micro-pits and grooves on the rubbed steel surfaces, thereby achieving the self-healing of the worn steel surface in association with the formation the boundary lubrication film thereon. The minimum WSD (0.49 mm) is achieved under the lubrication of RO with 0.3% Ni nanoparticles prepared at 200 °C (reduced by about 36%, as compared with 0.77 mm, the WSD under the lubrication of RO alone). After the reaction temperature exceeds 200 °C, the as-synthesized Ni nanoparticles exhibit similar antiwear performance. Therefore, the optimal reaction temperature for preparing nickel nanoparticles is 200 °C.

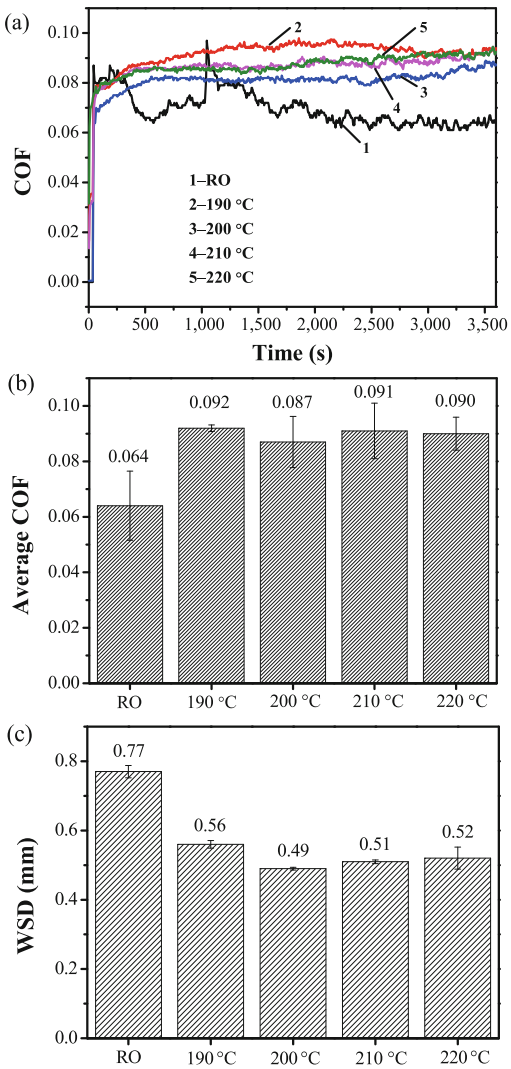

Fig. 8 COFs and WSDs of steel–steel contact lubricated by rapeseed oil with 0.3% Ni nanoparticles prepared at different reaction temperatures: (a) COF vs. time, (b) average COFs, and (c) average WSDs (four-ball machine, load: 392 N; rotation speed: 1,200 r/min; temperature: 75 °C; additive concentration: 0.3%; and sliding duration: 3,600 s).

Figure 9 depicts the variations in the COF and WSD of the steel–steel contact lubricated by the RO containing 0.3% Ni nanoparticles with the reaction time (the reaction temperature is fixed at 200 °C). As compared with the COF–time curve of the steel–steel sliding pair lubricated by RO alone, the COF–time curves of the same frictional pair lubricated by RO with 0.3% Ni nanoparticles obtained at reaction time of 30, 60, 90, 120, 150, and 180 min remain relatively high and stable (Fig. 9(a)). The average COF increases from 0.064 (for RO alone) to 0.094 for RO with 0.3% Ni nanoparticles (Fig. 9(b)). Furthermore, the Ni nanoparticles *in-situ* synthesized under different reaction time can also improve the antiwear performance of the RO base oil for the steel–steel contact, similar to those fabricated under different reaction temperatures. Here, the minimum WSD emerges under the lubrication of RO with 0.3% Ni nanoparticles obtained at a reaction

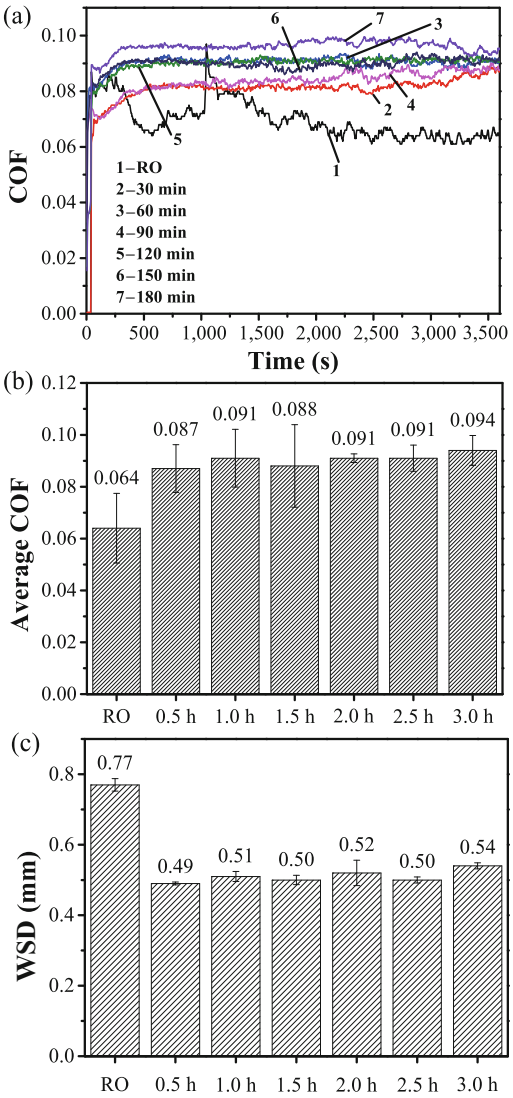

Fig. 9 COFs and WSDs of steel–steel contact under lubrication of rapeseed oil containing 0.3% Ni nanoparticles obtained at different reaction time: (a) COF vs. time, (b) average COFs, and (c) average WSDs (the sliding conditions are the same as those of Fig. 8, except for reaction time of 30–180 min with an interval of 30 min).

time of 30 min, which implies that the optimal reaction time for the *in-situ* synthesis of Ni nanoparticles in RO could be recommended as 30 min. In general, the Ni nanoparticles *in-situ* obtained in the RO base oil under different reaction duration exhibit similar antiwear ability, but that obtained at extended reaction duration of 3 h has relatively poor antiwear ability. This could be due to the Ostwald ripening phenomenon of Ni nanoparticles upon prolonged growth: The Ni nanoparticles grown at extended reaction duration would have a slightly increased particle size (Fig. S2 in the ESM), thereby adding to the abrasive wear of the steel–steel sliding pair.

Figure 10 shows the COFs and WSDs of the steel–steel contact lubricated by RO containing different concentrations of Ni nanoparticles *in-situ* synthesized under the optimal reaction condition (200 °C and 30 min). The COFs under the lubrication of RO with 0.1%, 0.5%, and 0.7% Ni nanoparticles are similar to that under the lubrication of RO alone (0.064). The COF under the lubrication of RO with 0.3% Ni nanoparticles is lower than that under the lubrication of RO alone in the first 350 s of the friction process,

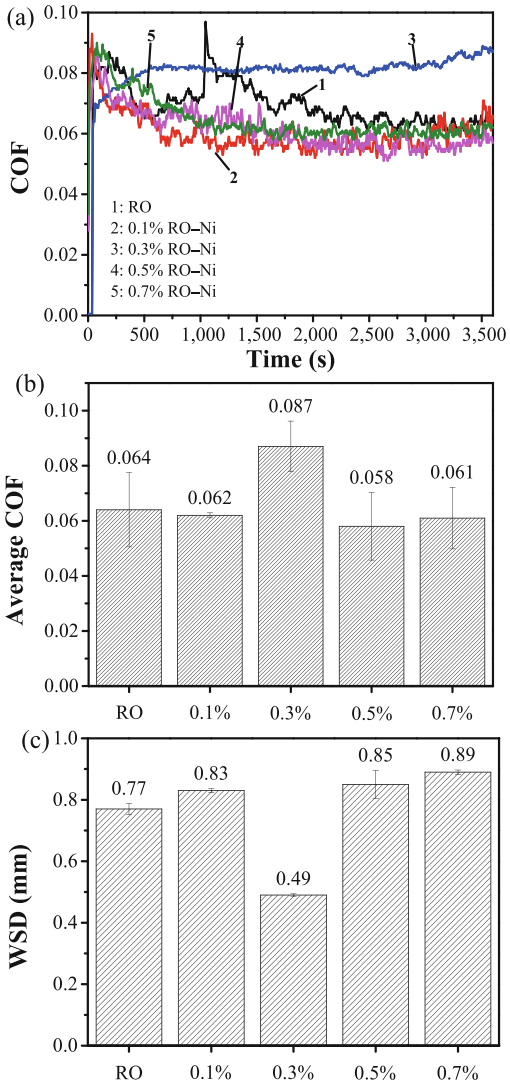

Fig. 10 COFs and WSDs of steel–steel contact lubricated by rapeseed oil containing different concentrations of nickel nanoparticles: (a) COF vs. time, (b) average COFs, and (c) average WSDs (the sliding conditions are the same as those of Fig. 8, except for additive concentrations of 0.1%, 0.3%, 0.5%, and 0.7%).

and then it gradually increases and stays at a high level of 0.087. Even worse, RO with 0.1%, 0.5%, and 0.7% Ni nanoparticles exhibit poorer antiwear ability than RO; and fortunately, RO with 0.3% Ni nanoparticles can significantly reduce the wear of the steel–steel contact. At this stage, we guess that the proper amount of Ni nanoparticles *in-situ* synthesized in RO can promote the occurrence of the tribochemical reaction on the rubbed steel surface, thereby influencing the lubrication behavior of the boundary lubrication film. Further research in this respect will be conducted in the following work.

Furthermore, the minimum oil film thickness (h_{min}) is estimated according to the well-known Hamrock–Dowson equation, as described by Eq. (2), where the h_{min} is dependent on various factors such as speed, applied load, and material parameter. The corresponding lubrication state can be approximately predicted according to the film thickness ratio (λ), as shown in Eq. (3). The h_{min} for RO calculated from Eq. (2) is 0.021 μm (for the specific calculation process, please see in Section S3 in the ESM). The surface roughness of the steel ball (R_{q_1} and R_{q_2}) are both 0.025 μm, and the λ for RO is calculated to be 0.7, which demonstrates that the steel–steel sliding pair lubricated by RO stays in the boundary lubrication regime.

$$h_{min} = 3.63R_x \frac{(G^*)^{0.49}(U^*)^{0.68}}{(W^*)^{0.073}}(1-e^{-0.68k}) \quad (2)$$

$$\lambda = \frac{h_{min}}{\sqrt{R_{q_1}^2 + R_{q_2}^2}} \quad (3)$$

In Eq. (2), R_x is the equivalent radius of the ball that can be described by the Hertz contact theory, G^* is the dimensionless material parameter, U^* is the dimensionless speed parameter, and W^* is the dimensionless load parameter. In addition, k is the contact ellipticity ratio, which is 1.03 in the four-ball test.

3.3 Analysis of worn surfaces

Figure 11 illustrates the SEM images and 3D topography of the wear scar on the lower steel balls lubricated by RO with 0.3% Ni nanoparticles prepared under the optimal reaction condition. The wear scar under the lubrication of RO alone is large and contains many wide and deep furrows and scratches (Fig. 11(a1–a3)), and the one under the lubrication of RO with 0.3% Ni nanoparticles is small and contains narrowed furrows as well as shallow scratches Fig. 11(b1–b3). The corresponding two-dimensional (2D) topography demonstrates that the wear scar under the lubrication of RO with 0.3% Ni nanoparticles is shallower and relatively smoother than that under the lubrication of RO alone oil (Fig. 12). Moreover, some small pits are visible on the wear scar lubricated by RO with 0.3% Ni nanoparticles, which could be due to a certain degree of abrasive wear caused by the aggregates of Ni nanoparticles under the Hall–Page effect [39].

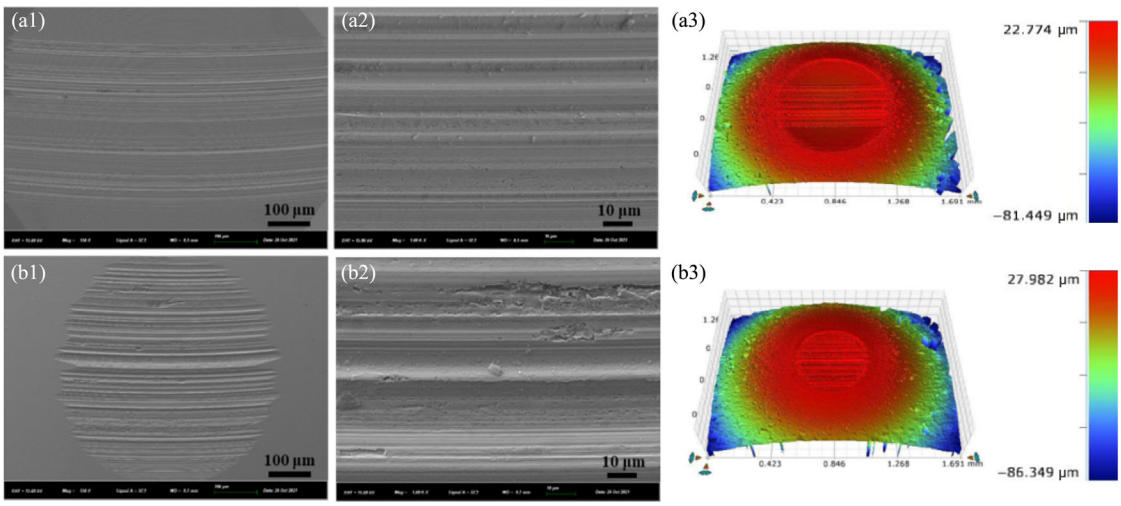

Fig. 11 SEM images (a1, a2, b1, b2) and 3D topography (a3, b3) of wear scars on lower steel ball lubricated by (a1–a3) rapeseed oil and (b1–b3) rapeseed oil with 0.3% Ni nanoparticle (the sliding conditions are the same as those of Fig. 8).

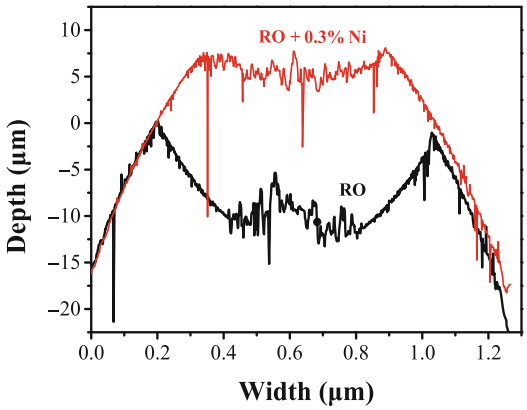

Fig. 12 2D topography of worn surface of lower steel ball (the sliding conditions are the same as those of Fig. 8).

Figure 13 presents the EDS element distributions on the wear scars under the voltage of 15 kV, which provides enough energy to excite electrons in the K shell of Ni, exhibiting greater intensity than the L line. As can be seen in Fig. 13(a), the O and C elements are present on the worn surface of the steel ball lubricated by RO alone, which indicates that the fatty acid components of neat RO can form the adsorbed film on the rubbed steel surface to reduce the friction and wear of the steel–steel sliding contact. Aside from the O and C elements, there is also a large amount of Ni element (5.58%) on the worn surface of the steel ball lubricated by RO with 0.3% Ni nanoparticles (Fig. 13(b) and Table 1). Furthermore, as seen in Fig. 13 and Table 1, there are C, O, and Ni elements enriched on the rubbed surface of the steel ball. This demonstrates that the lubricant consisting of RO and *in-situ* prepared Ni nanoparticles can form an adsorbed film composed of C, O, and Ni elements with good coverage on the rubbed steel surface.

The cross-sectional tribofilm on the worn steel surface lubricated by RO containing 0.3% nickel nanoparticles is further analyzed by the TEM–EDS. As shown in Fig. 14(a), the tribofilm is continuous and has a thickness of about 85 nm. The high-resolution TEM (HRTEM) image of region m in Fig. 14(a) is shown in Fig. 14(b), where region A, the carbon-rich layer, is of an amorphous structure, and the nanocrystals in region B exhibit spacings of 0.21 and 0.24 nm, corresponding to the (111) planes of nickel and nickel oxide, respectively. Besides, the nanocrystal with an interplanar spacing of 0.39 nm refers to the crystalline carbon structure. The corresponding line scan (along the direction from the Pt protective layer to the steel substrate) and surface scan of area n in Fig. 14(a) are shown in Figs. 14(c)–14(e). In Figs. 14(c) and 14(d), the line scan area is divided into four regions: Region I refers to the Pt protective layer,

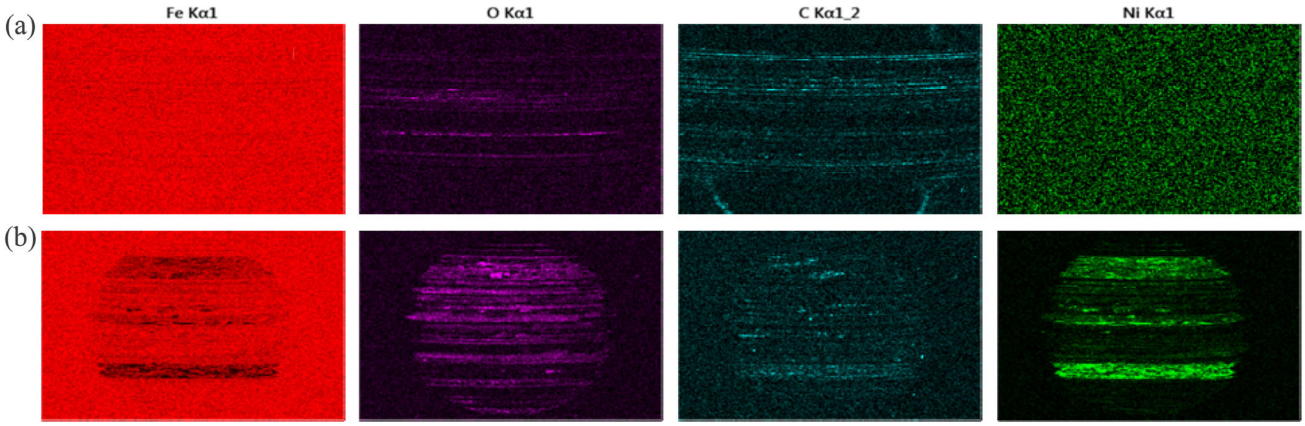

Fig. 13 EDS element surface distributions on rubbed steel surfaces (lower balls) lubricated by (a) rapeseed oil and (b) rapeseed oil with 0.3% Ni nanoparticle (the sliding conditions are the same as those of Fig. 8).

Table 1 Element compositions of rubbed steel surface lubricated by RO and RO with 0.3% Ni nanoparticle.

Lubricant	Element composition (%)				
	C	O	Fe	Ni	Others
RO	6.23	0.72	93.05	0	0
RO + 0.3% Ni	6.26	2.01	85.88	5.58	0.27

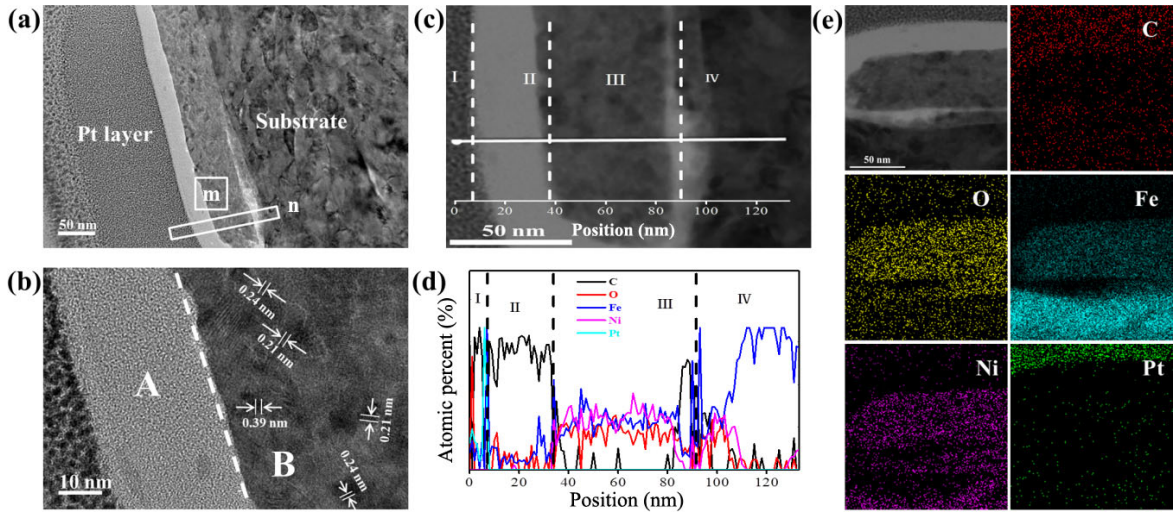

Fig. 14 TEM and EDS images of wear scar cross sections of lower steel ball lubricated by rapeseed oil containing 0.3% nickel nanoparticles: (a) TEM image of cross-sectional tribofilm, (b) HRTEM image of tribofilm, (c) line scan of major elements inside the tribofilm, (d) surface scans of elements inside the tribofilm, and (e) atomic distributions of elements across the tribofilm (the sliding conditions are the same as those of Fig. 8).

region II refers to the carbon layer with a relatively high and stable content of C as well as low contents of Fe, O, and Ni, and region III corresponds to the tribofilm (Fig. 14(c)). As compared with region II, region III has a relatively low content of C and high contents of O and Ni, possibly due to the generation of metal oxides during the friction process. Moreover, there are high contents of Ni and O as well as Fe in region IV, which could be due to the adsorption of the lubricant and its tribochemical reactions with atmospheric O and steel substrate therein (Fig. 14(c)). The element surface distribution maps are presented in Fig. 14(e), where the tribofilm mainly consists of Ni, O, Fe, and C, and the distribution of the elements are consistent with the results of the surface scan (Fig. 14(d)).

From Section 3.3, it can be concluded that an amorphous carbon film is formed by the carbonization of the base oil under the *in-situ* catalyzed of Ni nanoparticles with high catalytic capacity and surface activity [20, 21]. The shear strength of the carbon film could be higher than that of the organic film formed by RO, resulting in a relatively higher COF. Moreover, the organic film formed by RO is thin and can hardly prevent the direct contact between the hard steel surfaces, which could account for the relatively poor antiwear ability of RO. On the contrary, RO–Ni as the lubricant additive can form a relatively thick (about 85 nm) composite tribofilm composed of physically (and/or chemically) adsorbed film, tribochemical reaction film, and amorphous carbon film. Therefore, RO–Ni can significantly reduce the wear of the steel–steel sliding pair. However, the relatively thick composite tribofilm increases the roughness of the metal surface, resulting in an increased COF. From these, we can see that the antiwear performance and COF are two different physical properties; they are somewhat related but not identical. The relationship depends on the factors such as the chemical composition, structure, and surface treatment of the material. For example, a common lubricating additive molybdenum dialkyldithiocarbamate (MoDTC) exhibits a low and stable COF in the PAO base oil, due to the formation of a MoS_2 nanocrystal film with low shear strength; its antiwear performance under the same conditions, however, is relatively poor [40, 41]. Contrary to the former, zinc dialkydithiophosphate (ZDDP) (a traditional lubricant additive), lanthanum borate nanosheets, and CeO_2 nanoparticles have excellent antiwear performance but relatively high COFs, due to their rapid formation of thick tribofilms [42, 43]. Therefore, it is necessary to comprehensively consider these factors and select appropriate additives to meet specific practical application requirements.

The worn surface of the steel ball lubricated by RO with 0.3% Ni nanoparticles is also characterized

by the high-resolution XPS spectroscopy in order to analyze the tribomechanism of Ni nanoparticles in the RO base oil. Figure 15 depicts the XPS spectra of typical elements on the worn steel surface. In Fig. 15(a), the C 1s peaks at 284.10, 284.80, 286.51, and 288.85 eV correspond to the C=C bond, C–C bond, C–O bond, and C=O bond, respectively [44]. In Fig. 15(b), the O 1s peaks at 529.90, 531.75, and 533.88 eV correspond to the metal oxides, carbonyl compounds, and carbon oxides, respectively [45]. The XPS data reveal that the polar fatty acid molecules of the RO are adsorbed on the rubbed steel surface to form an adsorbed film [46]. The Fe 2p peaks at 706.83 eV (Fe $2p_{3/2}$) and 719.63 eV (Fe $2p_{1/2}$) are assigned to zero-valent Fe coming from the steel ball (Fig. 15(c)), the Fe 2p peaks at 709.64 eV (Fe $2p_{3/2}$) and 722.17 eV (Fe $2p_{1/2}$) are attributed to FeO [47], and those Fe 2p peaks at 711.10 eV (Fe $2p_{3/2}$) and 723.44 eV (Fe $2p_{1/2}$) are assigned to Fe_2O_3 [43, 47, 48]. These XPS data indicate that the steel substrate and atmospheric O participate in tribochemical reactions under the friction-induced local high temperatures and high contact stress [49, 50]. The Ni 2p peaks at 852.69 eV (Ni $2p_{3/2}$) and 869.94 eV (Ni $2p_{1/2}$) are ascribed to zero-valent Ni (Fig. 15(d)), which indicates that the *in-situ* synthesized Ni nanoparticles are adsorbed on the rubbed steel surface, thereby filling up the micro-pits or grooves thereon. In addition, the Ni 2p peaks at 855.57 eV (Ni $2p_{3/2}$) and 873.05 eV (Ni $2p_{1/2}$) are ascribed to Ni_2O_3 [51, 52], which indicates that a part of Ni nanoparticles participate in tribochemical reactions with atmospheric oxygen to form a tribochemical reaction film. On the one hand, nickel nanoparticles can be deposited on the steel surface to self-heal the worn surface. On the other hand, they take part in tribochemical reactions with atmospheric O and substrate Fe to form a tribofilm mainly composed of iron and nickel oxides as well as adsorbed polar species of RO. This could well explain why Ni nanoparticles *in-situ* synthesized in RO with a proper dosage can reduce the friction and wear of the steel–steel sliding contact at a certain degree.

As mentioned in Section 3.3, the tribomechanism of the as-synthesized nickel nanoparticles in RO is schematically illustrated in Fig. 16. The nickel nanoparticles *in-situ* synthesized in the RO exhibit good dispersion stability as well as uniformity, thanks to the encapsulation by the free polar fatty acid molecules of RO. During the friction test, a part of Ni nanoparticles and the polar organic species of RO

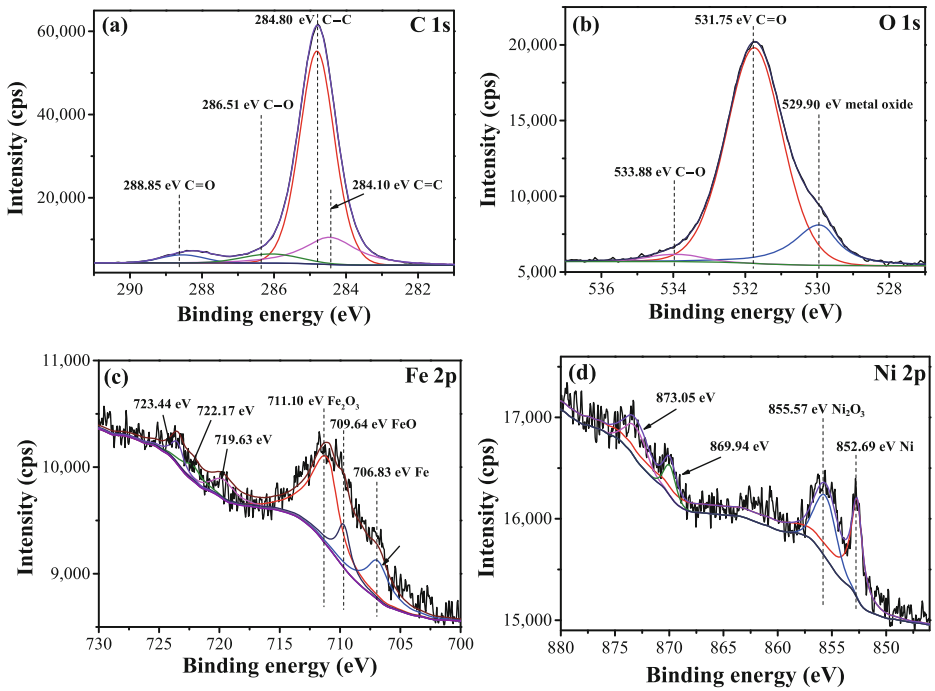

Fig. 15 XPS spectra of typical elements on worn surface of lower steel ball under lubrication of rapeseed oil with 0.3% Ni nanoparticles (the sliding conditions are the same as those of Fig. 8).

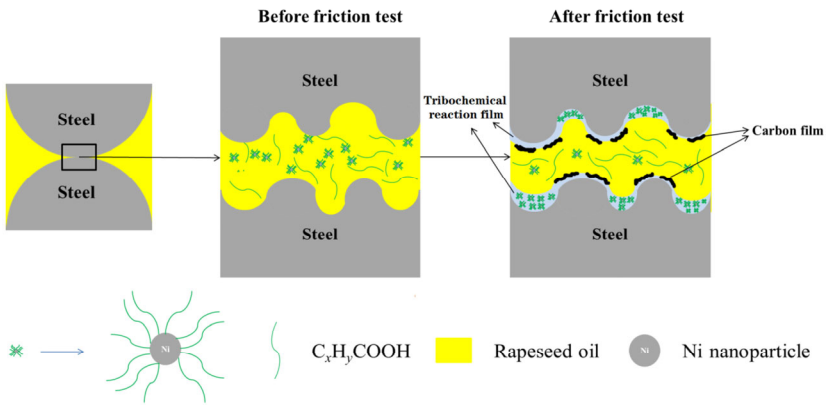

Fig. 16 Schematic diagram illustrating tribomechanism of nickel nanoparticles in rapeseed oil.

are deposited and adsorbed in the contact area of the sliding pair, which contributes to preventing the direct contact between the sliding surfaces and self-healing the micro-pits thereon with the assistance of magnetic attraction. At the same time, some nickel nanoparticles participate in tribochemical reactions with atmospheric O and steel substrate under high-speed sliding to form a tribofilm composed of C, O, Ni, and Fe elements. Furthermore, an amorphous carbon film is formed via the carbonization of base oil under the catalysis of Ni nanoparticles. Due to the formation of thick tribofilm and rough friction surface, the COF increases, however, the adsorption layer, the tribochemical reaction film, and carbon layer jointly function to greatly enhance the antiwear performance of the RO for the steel–steel contact.

4 Conclusions

Ni nanoparticles are *in-situ* synthesized in RO through the reduction of nickel acetylacetonate therein. Using RO as the surface modifier, reducing agent, and solvent, the present approach is facile and environmentally acceptable, and it can afford Ni nanoparticles possessing good compatibility with vegetable oil. The Ni nanoparticles *in-situ* synthesized under the optimized reaction condition (200 °C and 30 min) have a uniform particle size distribution as well as good monodispersity, oil solubility, and dispersion stability. Besides, the RO with 0.3% *in-situ* synthesized Ni nanoparticles exhibits good antiwear performance for the steel–steel contact. This is because the Ni nanoparticles can be deposited on the rubbed steel surface to fill up and/or repair the micro-pits and grooves. In the meantime, they also participate in tribochemical reactions with atmospheric O and substrate Fe under the boundary lubrication condition to form a tribochemical reaction film composed of fatty acids as well as the oxides of iron and nickel. In addition, under the catalysis of Ni nanoparticles, the base oil on the contact surface is carbonized to form an amorphous carbon film. The adsorbed layer, the tribochemical reaction film, and the amorphous carbon layer comprise the composite tribofilm to keep off the rubbed steel surfaces and reduce their friction and wear.

Acknowledgements

The authors acknowledge the financial support provided by the National Natural Science Foundation of China (Grant Nos. 51875172 and 52105180), Zhongyuan Science and Technology Innovation Leadership Program (Grant No. 214200510024), the Tribology Science Fund of State Key Laboratory of Tribology in Advanced Equipment (Grant No. SKLTKF21B06), and Key Research and Development and Promotion Projects in Henan Province (Grant Nos. 212102310410, 232102230067, and 232102230081).

Declaration of competing interest

The authors have no competing interests to declare that are relevant to the content of this article. The author Jun XU is the Communication Editor of this journal.

Electronic Supplementary Material

Supplementary material is available in the online version of this article at https://doi.org/10.1007/s40544-023-0776-0.

References

[1] Rasep Z, Muhammad Yazid M N A W, Samion S. Lubrication of textured journal bearing by using vegetable oil: A review of approaches, challenges, and opportunities. *Renew Sust Energ Rev* **146**: 111191 (2021)

[2] Singh R. Progress of environment friendly cutting fluids/solid lubricants in turning—A review. *Mater Today* **37**: 3577–3580 (2021)

[3] Ranjan N, Shende R C, Kamaraj M, Ramaprabhu S. Utilization of TiO_2/gC_3N_4 nanoadditive to boost oxidative properties of vegetable oil for tribological application. *Friction* **9**(2): 273–287 (2021)

[4] Xu Z, Lou W J, Zhao G Q, Zhang M, Hao J Y, Wang X B. Pentaerythritol rosin ester as an environmentally friendly multifunctional additive in vegetable oil-based lubricant. *Tribol Int* **135**: 213–218 (2019)

[5] Ferreira E N, Arruda T B M G, Rodrigues F E A, Moreira D R, Chaves P O B, da Silva Rocha W, da Silva L M R, Petzhold C L, Ricardo N M P S. Pequi oil esters as an alternative to environmentally friendly lubricant for industrial purposes. *ACS Sustainable Chem Eng* **10**(3): 1093–1102 (2022)

[6] Shill D C, Das A K, Chatterjee S. Lightning impulse breakdown performance of saturated vs unsaturated vegetable oil and their mixtures with mineral oil. *Ind Crop Prod* **184**: 115044 (2022)

[7] Xu M, Yu X, Ni J. Penetration and lubrication evaluation of vegetable oil with nanographite particles for broaching process. *Friction* **9**(6): 1406–1419 (2021)

[8] Long Y, Wang Y, Weihnacht V, Makowski S, Kubo M, Martin J M, de Barros Bouchet M I. Mechanism of superlubricity of a DLC/Si_3N_4 contact in the presence of castor oil and other green lubricants. *Friction* **10**(10): 1693–1706 (2022)

[9] Ali M K A, Hou X J. Improving the tribological behavior of internal combustion engines via the addition of nanoparticles to engine oils. *Nanotechnol Rev* **4**(4): 347–358 (2015)

[10] Bin Mustafa M M, Umehara N, Tokoroyama T, Murashima M, Shibata A, Utsumi Y, Moriguchi H. Effect of mesh structure of tetrahedral amorphous carbon (ta-C) coating on friction and wear properties under base-oil lubrication condition. *Tribol Int* **147**: 105557 (2020)

[11] Meng Y G, Xu J, Jin Z M, Prakash B, Hu Y Z. A review of recent advances in tribology. *Friction* **8**(2): 221–300 (2020)

[12] Uflyand I E, Zhinzhilo V A, Burlakova V E. Metal-containing nanomaterials as lubricant additives: State-of-the-art and future development. *Friction* **7**(2): 93–116 (2019)

[13] Karthikeyan K M B, Vijayanand J, Arun K, Rao V S. Thermophysical and wear properties of eco-friendly nano lubricants. *Mater Today* **39**: 285–291 (2021)

[14] Alves S M, Barros B S, Trajano M F, Ribeiro K S B, Moura E. Tribological behavior of vegetable oil-based lubricants with nanoparticles of oxides in boundary lubrication conditions. *Tribol Int* **65**: 28–36 (2013)

[15] Chen B S, Gu K C, Fang J H, Wu J, Wang J, Zhang N. Tribological characteristics of monodispersed cerium borate nanospheres in biodegradable rapeseed oil lubricant. *Appl Surf Sci* **353**: 326–332 (2015)

[16] Jiang Z Q, Zhang Y J, Yang G B, Ma J Y, Zhang S M, Yu L G, Zhang P Y. Tribological properties of tungsten disulfide nanoparticles surface-capped by oleylamine and maleic anhydride dodecyl ester as additive in diisooctylsebacate. *Ind Eng Chem Res* **56**(6): 1365–1375 (2017)

[17] Jiang Z Q, Zhang Y J, Yang G B, Yang K P, Zhang S M, Yu L G, Zhang P Y. Tribological properties of oleylamine-modified ultrathin WS_2 nanosheets as the additive in polyalpha olefin over a wide temperature range. *Tribol Lett* **61**(3): 24 (2016)

[18] Meng Y, Su F H, Chen Y Z. Nickel/multi-walled carbon nanotube nanocomposite synthesized in supercritical fluid as efficient lubricant additive for mineral oil. *Tribol Lett* **66**(4): 134 (2018)

[19] Tu Z Q, Hu E Z, Wang B B, David K D, Seeger P, Moneke M, Stengler R, Hu K H, Hu X G. Tribological behaviors of Ni-modified citric acid carbon quantum dot particles as a green additive in polyethylene glycol. *Friction* **8**(1): 182–197 (2020)

[20] Hu J S, Zhang Y J, Yang G B, Gao C P, Song N N, Zhang S M, Zhang P Y. *In-situ* formed carbon based composite tribo-film with ultra-high load bearing capacity. *Tribol Int* **152**: 106577 (2020)

[21] Hu J S, Wang C F, Zhang P Y, Zhang S M, Zhang Y J. Diisooctyl sebacate-containing nickel nanoparticles for lubrication of steel sliding parts under magnetic fields. *ACS Appl Nano Mater* **4**(7): 7007–7016 (2021)

[22] Cho Y S, Moon J W, Chung K C, Lee J G. Synthesis of nickel and copper nanopowders by plasma arc evaporation. *Joural of Korean Power Metallurgy Institute* **20**(6): 411–424 (2013)

[23] Liu Y F, Zhu K L, Li X L, Lin F M, Li Y. Analysis of multi-scale Ni particles generated by ultrasonic aided electrical discharge erosion in pure water. *Adv Powder Technol* **29**(4): 863–873 (2018)

[24] Panigrahi B B, Das K, Godkhindi M M. Dilatometry of ball milled nickel nano powder during non-isothermal sintering. *Sci Sinter* **39**(1): 25–29 (2007)

[25] Logutenko O A, Titkov A I, Vorob'yov A M, Balaev D A, Shaikhutdinov K A, Semenov S V, Yukhin Y M, Lyakhov N Z. Effect of molecular weight of sodium polyacrylates on the size and morphology of nickel nanoparticles synthesized by the modified polyol method and their magnetic properties. *Eur Polym J* **99**: 102–110 (2018)

[26] Guo K, Li H L, Yu Z X. Size-dependent catalytic activity of monodispersed nickel nanoparticles for the hydrolytic dehydrogenation of ammonia borane. *ACS Appl Mater Interfaces* **10**(1): 517–525 (2018)

[27] Park J, Joo J, Kwon S, Jang Y, Hyeon T. Synthesis of monodisperse spherical nanocrystals. *Angew Chem Int Ed* **46**(25): 4630–4660 (2007)

[28] Murru C, Badía-Laíño R, Díaz-García M E. Oxidative stability of vegetal oil-based lubricants. *ACS Sustainable Chem Eng* **9**(4): 1459–1476 (2021)

[29] Mao X H, Zhao X Z, Huyan Z Y, Liu T T, Yu X Z. Relationship of glucosinolate thermal degradation and roasted rapeseed oil volatile odor. *J Agric Food Chem* **67**(40): 11187–11197 (2019)

[30] Bridges D, Xu R, Hu A M. Microstructure and mechanical properties of Ni nanoparticle-bonded Inconel 718. *Mater Design* **174**: 107784 (2019)

[31] Bhattacharjee D, Sheet S K, Khatua S, Biswas K, Joshi S, Myrboh B. A reusable magnetic nickel nanoparticle based catalyst for the aqueous synthesis of diverse heterocycles and their evaluation as potential anti-bacterial agent. *Bioorg Med Chem* **26**(18): 5018–5028 (2018)

[32] Pan Y, Jia R R, Zhao J C, Liang J L, Liu Y Q, Liu C G. Size-controlled synthesis of monodisperse nickel nanoparticles and investigation of their magnetic and catalytic properties. *Appl Surf Sci* **316**: 276–285 (2014)

[33] Shukla N, Liu C, Jones P M, Weller D. FTIR study of surfactant bonding to FePt nanoparticles. *J Magn Magn Mater* **266**(1–2): 178–184 (2003)

[34] Söderlind F, Pedersen H, Petoral R M, Käll P O, Uvdal K. Synthesis and characterisation of Gd_2O_3 nanocrystals functionalised by organic acids. *J Colloid Interf Sci* **288**(1): 140–148 (2005)

[35] Yang K, Peng H B, Wen Y H, Li N. Re-examination of characteristic FTIR spectrum of secondary layer in bilayer oleic acid-coated Fe_3O_4 nanoparticles. *Appl Surf Sci* **256**(10): 3093–3097 (2010)

[36] Huang X J, Chen Y B, Feng X S, Hu X Y, Zhang Y F, Liu L. Incorporation of oleic acid-modified Ag@ZnO core–shell nanoparticles into thin film composite membranes for enhanced antifouling and antibacterial properties. *J Membr Sci* **602**: 117956 (2020)

[37] Santos J C O, Santos I M G, Conceição M M, Porto S L, Trindade M F S, Souza A G, Prasad S, Fernandes V J, Araújo A S. Thermoanalytical, kinetic and rheological parameters of commercial edible vegetable oils. *J Therm Anal Calorim* **75**(2): 419–428 (2004)

[38] Fan K Z, Li J, Ma H B, Wu H, Ren T H, Kasrai M, Bancroft G M. Tribological characteristics of ashless dithiocarbamate derivatives and their combinations with ZDDP as additives in mineral oil. *Tribol Int* **41**(12): 1226–1231 (2008)

[39] Wang L P, Gao Y, Xu T, Xue Q J. A comparative study on the tribological behavior of nanocrystalline nickel and cobalt coatings correlated with grain size and phase structure. *Mater Chem Phys* **99**(1): 96–103 (2006)

[40] Zhang S J, Zhu L N, Wang Y Y, Kang J J, Wang H D, Ma G Z, Huang H P, Zhang G A, Yue W. Effects of annealing treatment on tribological behavior of tungsten-doped diamond-like carbon film under lubrication (Part 2): Tribological behavior under MoDTC lubrication. *Friction* **10**(7): 1061–1077 (2022)

[41] Spikes H. Friction modifier additives. *Tribol Lett* **60**(1): 5 (2015)

[42] Wu J, Yang G B, Zhang S M, Zhang Y J, Sun L, Sun T H, Yu L G, Zhang P Y. Preparation of nanofluid of lanthanum borate nanosheets and investigation of its tribological properties and tribomechanisms in different base oils. *Tribol Lett* **71**(1): 1 (2023)

[43] Lei X, Zhang Y J, Zhang S M, Yang G B, Zhang C L,

Zhang P Y. Study on the mechanism of rapid formation of ultra-thick tribofilm by CeO_2 nano additive and ZDDP. *Friction* **11**(1): 48–63 (2023)

[44] Huang W J. Tribological properties of benzothiazole derivatives as additives in rapeseed oil. *Tribology* **23**(1): 33–37 (2003) (in Chinese)

[45] Xu N, Zhang M, Li W M, Zhao G Q, Wang X B, Liu W M. Study on the selectivity of calcium carbonate nanoparticles under the boundary lubrication condition. *Wear* **307**(1–2): 35–43 (2013)

[46] Jiang Z Q, Fang J H, Chen F, Feng Y H, Wang X, Chen B S, Gu K C, Liu P. Tribological properties of rapeseed oil with electromagnetic field impact. *Tribology* **38**(1): 44–50 (2018) (in Chinese)

[47] Gong K L, Lou W J, Zhao G Q, Wu X H, Wang X B. MoS_2 nanoparticles grown on carbon nanomaterials for lubricating oil additives. *Friction* **9**(4): 747–757 (2021)

[48] Xiong S, Zhang B S, Luo S, Wu H, Zhang Z. Preparation, characterization, and tribological properties of silica-nanoparticle-reinforced B–N-co-doped reduced graphene oxide as a multifunctional additive for enhanced lubrication. *Friction* **9**(2): 239–249 (2021)

[49] Wang B B, Hu E Z, Tu Z Q, David K D, Hu K H, Hu X G, Yang W, Guo J H, Cai W M, Qian W L, et al. Characterization and tribological properties of rice husk carbon nanoparticles Co-doped with sulfur and nitrogen. *Appl Surf Sci* **462**: 944–954 (2018)

[50] Huang J, Li Y, Jia X H, Song H J. Preparation and tribological properties of core–shell Fe_3O_4@C microspheres. *Tribol Int* **129**: 427–435 (2019)

[51] Wang J B, Zhang H, Hu W J, Li J S. Tribological properties and lubrication mechanism of nickel nanoparticles as an additive in lithium grease. *Nanomaterials* **12**(13): 2287 (2022)

[52] Liu Y H, Xin L, Zhang Y J, Chen Y F, Zhang S M, Zhang P Y. The effect of Ni nanoparticles on the lubrication of a DLC-based solid–liquid synergetic system in all lubrication regimes. *Tribol Lett* **65**(2): 31 (2017)

Wenya XU. He received his bachelor's degree in materials science and engineering in 2018 from Henan University of Urban Construction, Pingdingshan, China. He was a master graduate student in Engineering Research Center for Nanomaterials, Henan University, Kaifeng, China. He obtained his Master's degree in materials science and engineering in 2022. His main research interests are the controlled synthesis of nickel nanoparticles and tribological properties in vegetable oils.

Guangbin YANG. He received his Ph.D. degree in condensed matter physics in 2011 from Henan University, Kaifeng, China. Now he is an associate professor in Henan University Kaifeng, China. His research areas cover the nanotribology, the lubricants, and nano-additives. He has published more than 70 journal papers and possesses three ministerial and provincial-level science and technology awards.

Pingyu ZHANG. He received his Ph.D. degree from Lanzhou Institute of Chemical Physics, Chinese Academy of Sciences, Lanzhou, China, in 2000. He joined Henan University, Kaifeng, China, in 2003, and now he is a professor and director of Engineering Research Center for Nanomaterials in Henan University, Kaifeng, China. His current research interests cover nanoparticle lubricant additives, high-performance lubricants and functional materials, and the tribology of materials. He has published over 130 journal papers and gained a number of ministerial and provincial-level science and technology awards.